Available online at www.sciencedirect.com

ScienceDirect

Advances in Space Research 70 (2022) 249–267

ADVANCES IN SPACE RESEARCH (a COSPAR publication)

www.elsevier.com/locate/asr

Copernicus Sentinel–1 POD reprocessing campaign

Marc Fernández [a,*], Heike Peter [b], Daniel Arnold [c], Bingbing Duan [d], Wim Simons [e], Martin Wermuth [f], Stefan Hackel [f], Jaime Fernández [a], Adrian Jäggi [c], Urs Hugentobler [d], Pieter Visser [e], Pierre Féménias [g]

[a] GMV AD., Tres Cantos, Spain
[b] PosiTim UG, Seeheim-Jugenheim, Germany
[c] Astronomical Institute, University of Bern, Bern, Switzerland
[d] Technische Universität München, Munich, Germany
[e] Delft University of Technology, Delft, The Netherlands
[f] DLR GSOC, Oberpfaffenhofen, Germany
[g] ESA/ESRIN, Largo Galileo Galilei 1, I-00044 Frascati, Italy

Received 17 December 2021; received in revised form 11 April 2022; accepted 13 April 2022
Available online 22 April 2022

Abstract

Copernicus Sentinel–1 is a C-Band Synthetic Aperture Radar (SAR) satellite mission within the European Copernicus Programme. The two satellites Sentinel-1A and -1B were launched in April 2014 and 2016, respectively. The Copernicus POD (Precise Orbit Determination) Service is responsible for the determination of orbital and auxiliary products required by the Payload Data Ground Segment (PDGS). Precise orbits are determined based on the dual-frequency GPS (Global Positioning System) data delivered by dedicated geodetic-grade GPS receivers on-board the satellites. Several updates in the operational orbit determination were done during the years including an update of the GPS antenna reference point coordinates. The switch to GPS carrier phase ambiguity-fixing was a major improvement. A reprocessing of the entire mission span of both satellites became necessary to provide a consistent orbit time series for the mission based on state-of-the-art models and processing settings. Due to the lack of independent observation techniques, the Sentinel-1 orbit quality has been assessed by analysing processing metrics, orbit overlaps and orbit comparisons. For this purpose, members of the Copernicus POD Quality Working Group (QWG) provided reprocessed Sentinel-1 orbit time series based on their software packages and their orbit determination settings. A weighted average of all five delivered solutions - a combined orbit - serves as reference for the comparisons. The quality and reliability of this reference orbit depends among others on the number of available orbit solutions and whether a manoeuvre has been performed during the processed day or not. The mean orbit consistency between all orbit solutions is below 1 cm in 3D RMS for the entire mission time interval for both satellites. Only few days show inferior quality due to data gaps or orbit manoeuvres. Following this sophisticated validation process, the reprocessed Sentinel-1 orbits from the Copernicus POD Service have been made available to the user community.

Keywords: GPS; Copernicus; Sentinel–1; Precise Orbit Determination; Reprocessing

1. Introduction

The European Copernicus programme (Aschbacher and Milagro-Pérez, 2012) consists of several satellite missions dedicated to various remote sensing techniques of planet Earth. The Copernicus Sentinel-1 mission (Fletcher, 2012;

* Corresponding author.
E-mail address: mffernandez@gmv.com (M. Fernández).

https://doi.org/10.1016/j.asr.2022.04.036
0273-1177/

Torres et al., 2012) is a C-Band Synthetic Aperture Radar (SAR) mission and the first mission in the programme. The SAR instrumentation is built on the heritage of the ASAR (Advanced SAR) instrument on Envisat (Louet, 2001). Fig. 1 shows an artist impression of the Sentinel-1 satellite. The two Sentinel-1 satellites (A and B) were launched in April 2014 and 2016, respectively. Precise orbits of the satellites are needed for the SAR processing. The orbit products are delivered by the Copernicus POD (Precise Orbit Determination) Service (Fernández et al., 2014). This service is a consortium led by GMV, Spain, being responsible for all operations. Additional members are:

- PosiTim UG, Germany
- Astronomical Institute of the University of Bern (AIUB), Switzerland
- German Space Operations Centre, *Deutsches Zentrum für Luft- und Raumfahrt* (DLR), Germany
- Faculty of Aerospace Engineering, Delft University of Technology (TUD), The Netherlands
- Institute for Physical and Astronomical Geodesy and German Geodetic Research Institute, Technical University of Munich (TUM), Germany
- *GeoForschungsZentrum* (GFZ), Germany

The Copernicus POD (CPOD) Service provides orbit and auxiliary products for the Copernicus Sentinel-1, -2, -3, and recently -6 missions to the Payload Data Ground Segments (PDGS). These products are also made available to the user community through the ESA (European Space Agency) Copernicus Open Access Hub (COAH)[1]. The orbital products have different latency and accuracy requirements. In the case of Sentinel-1, the most stringent accuracy requirement is given for the Non-Time Critical (NTC) orbit product. The orbit accuracy requirement is given as a maximum of 5 cm in 3D RMS in the comparison to external processing facilities (GMES Sentinel-1 Team, 2010). This requirement is well fulfilled by the operational orbital products generated by the CPOD Service. The reports from the Regular Service Review[2] (RSR) generated every three months show a consistency between all delivered orbit solutions of maximum 1 cm in 3D RMS for the Sentinel-1 orbits (GMV, 2021). The CPOD Service is committed to deliver satellite orbit solutions based on state-of-the-art models and processing standards. Therefore, the operational orbit determination settings are updated from time to time (Peter and GMV team, 2021). As a consequence, the orbit time series generated operationally are not consistent for the entire mission span.

Various analyses have been performed during the last years to especially improve the orbit quality and consistency for Sentinel-1 satellites. At first, a correction of the Up-component of the antenna Phase Centre Offset (PCO) by 3 cm improved the radial orbit consistency significantly (Peter et al., 2017). Secondly, a correction of erroneous GPS (Global Positioning System) Antenna Reference Point (ARP) coordinates and the additional estimation of corrections to the vector between the centre of mass of the satellite and the GPS antenna phase centre (Peter et al., 2020a, Fernández et al., 2019) led to a major update of the processing set-up at the end of July 2020 (Peter and GMV team, 2021). Table 1 summarises the mentioned evolutions carried out in the ARP coordinates and PCO values.

Fig. 1. Sentinel-1 satellite (copyright: ESA/ATG Medialab).

Fig. 2 shows the daily 3D RMS of the orbit differences between the former operational CPOD solutions and the reprocessed orbit solutions for both Sentinel-1 satellites. The large jumps of 6–7 cm in the orbits due to the correction of the ARP and PCO made the reprocessing definitely necessary. In addition to this major change, the orbit parametrisation has recently been reviewed for the first three Sentinel missions as well (Peter et al., 2020b). The main changes on the orbit parametrisation are: (a) the estimation of 16 constant-per-revolution (CPR) parameters with stronger constraint (old: $\sigma = 0.01$ m/s^2; new: $\sigma = 1$ 0 nm/s^2 (sine + cosine) and $\sigma = 1$ nm/s^2 (constant)) instead of the previous 3 estimated CPRs (constant CPRs in both along-track and cross-track directions have also been added to the estimation), (b) the satellite radiation pressure coefficient has been fixed to value 1.0 instead of being estimated during the processing of each orbit product, and (c) only 1 drag scale factor is currently estimated instead of the 15 from previous scheme. The switch to the new parametrisation was performed in mid-January 2021 for the operational orbit determination (Peter and GMV team, 2021).

The GPS-based orbit determination for the Sentinel-1 satellites needs information about the precise GPS orbit and clock products directly or from members of the International GNSS Service (IGS, Johnston et al., 2017). The CPOD Service used IGS final products for the processing of their own operational products until the switch to the single-receiver ambiguity resolution, also known as PPP-AR (Precise Point Positioning Ambiguity

[1] https://scihub.copernicus.eu/.
[2] https://sentinel.esa.int/web/sentinel/technical-guides/sentinel-1-sar/pod/documentation.

Table 1
Evolution and current ARP coordinates and PCO values of Sentinel-1 satellites.

	Satellite	Antenna	Initial values [mm]			Change on 25/09/2015[1] [mm]			Current values[2] [mm] (change on 28/07/2020)		
			X	Y	Z	X	Y	Z	X	Y	Z
ARP[3]	S-1A / S-1B	GPSA[5]	−976.2	286.9	124.1	–	–	–	−937.1	332.1	131.0
		GPSB[5]	−985.5	513.5	229.3	–	–	–	−946.5	558.7	236.2
PCO[4]	S-1A	GPSA	1.00	−0.50	99.50	−0.50	1.00	68.00	−1.98	−11.22	59.80
		GPSB	1.00	−0.50	99.50	−0.50	1.00	68.00	−1.98	−11.22	59.80
	S-1B	GPSA	–	–	–	−0.50	1.00	68.00	−3.48	−21.13	51.92
		GPSB[6]	–	–	–	−0.50	1.00	68.00	−3.48	−21.13	51.92

(1) Sentinel-1B adopted these PCO values from the beginning of the mission.
(2) These ARP coordinated and PCO values have been used for all centres and the entire Sentinel-1 reprocessing campaign.
(3) ARP coordinates are referring to the satellite body-fixed system explained in detail in Peter et al. (2017).
(4) PCO values are referring to the antenna reference frame explained in detail in Peter et al. (2017); the ANTEX file uses the convention Y/X/Z (left-handed system).
(5) The GPSA antenna is the nominal antenna, whereas the GPSB antenna is the redundant antenna for both ARP and PCO.
(6) Sentinel-1B GPSB receiver has never been switched on.

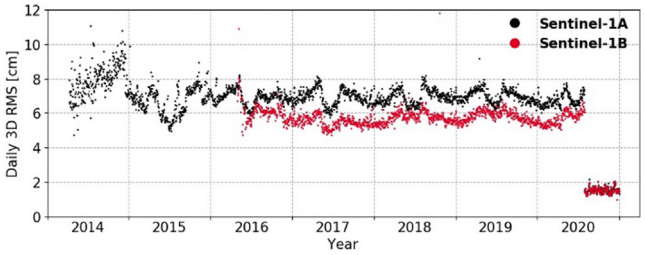

Fig. 2. Orbit comparisons [daily 3D RMS, cm] between the former Sentinel-1 operational CPOD Service solutions and the current reprocessed solutions over time. Note the jump in 2020 due to updated values for the GPS antenna location.

Resolution), carried out in mid-July 2020. This method has already been applied successfully to other Sentinel satellites, e.g., Sentinel-3 (Montenbruck et al., 2018, Mao et al., 2021, Duan and Hugentobler, 2021) and Sentinel-6 (Montenbruck et al., 2021). The so-called bias products consistent to the corresponding orbit and clock products are needed to account for GPS satellite-specific biases in PPP-AR. Such consistent product sets are available from various analysis centres of the IGS. The CPOD Service selected the final products from CODE (Center for Orbit Determination in Europe, Dach et al., 2020), which consist of orbits, clocks and observation-specific biases (Schaer et al., 2021) to perform PPP-AR for the operational CPOD orbit determination processing.

On 29th January 2017, IGS switched between reference frames IGb08 and IGS14 for their products (Rebischung, 2016; Rebischung and Schmid, 2016). On 17th May 2020, the switch to IGb14 followed (Rebischung, 2020). To avoid inconsistencies, the Sentinel-1 orbit reprocessing has used IGb14 as a reference frame. GPS products based on this reference frame and for the entire Sentinel-1 mission time have been provided by CODE, which generated a consistent reprocessed time series of their products (Villiger et al., 2020).

Sentinel-1 satellites are not equipped with an additional observation technique allowing for independent validation of the POD results (e.g., Sentinel-3 satellites have a laser retro reflector for Satellite Laser Ranging and a DORIS, *Détermination d'Orbite et Radiopositionnement Intégré par Satellite*, receiver). No independent measurements are therefore available to validate the GPS-derived orbit determination results. Verification of the POD results is possible by comparing to orbit solutions from other institutions and by doing analysis of orbit overlaps and processing metrics. External orbit solutions are delivered from members of the Copernicus POD Quality Working Group (QWG). The QWG is part of the CPOD Service (Fernández et al., 2014). ESA and Eumetsat (European Organisation for the Exploitation of Meteorological Satellites) are chairing the group together. Members of the group are representatives of Mission Processing Centres, PDGS, and Post-Launch Support from each Sentinel mission. The QWG is administered and organised by GMV and PosiTim. Next

to these two institutions, the core of the QWG is built by institutions with a long LEO (Low Earth Orbit) POD expertise (Allahvirdi-Zadeh et al., 2022): AIUB, DLR, TUD, TUM, and European Space Operations Centre (ESOC), Germany. Some other institutions such as CNES (*Centre National d'Études Spatiales*), GRGS (*Groupe de Recherche de Géodésie Spatiale*), JPL (Jet Propulsion Laboratory), GSFC (Goddard Space Flight Center) and GFZ are also QWG members but their contributions only focus on Sentinel-3 and Sentinel-6 missions.

The above mentioned core members of the QWG have all contributed to the Sentinel-1 reprocessing and have delivered orbits for the full mission intervals for the two Sentinel-1 satellites. ESOC provided independent analysis to the Sentinel-1 reprocessing, which was not included in this publication. All other orbit solutions have been used together with the CPOD solution to generate a combined orbit based on a weighted average. This combined orbit served as a reference to validate the quality of the different orbit solutions, primarily of the reprocessed CPOD orbits before they have been distributed to the user community through the ESA COAH. The improvement of reprocessed orbits with respect to the former operational orbit solutions has already been noticed in the application of Sentinel-1 SAR along-track sub-pixel offsets for determining horizontal velocities in a global reference frame, with the average RMSE of the offsets improved by 4.7 mm, or 13 % (Lazecky and Hooper, 2022).

Following this introduction, Section 2 provides a data description complementing the information given within this section. Section 3 describes the different POD processing strategies of the involved institutions. The results of the reprocessing campaign are analysed in detail in Section 4. A particular case study involving a particle impact on Sentinel-1A satellite is also addressed at the end of this section. The article is closed with a summary and conclusion section (Section 5).

2. DATA description

The reprocessing is based on nearly all GPS data available for the two Sentinel-1 satellites until the end of year 2020. The orbit reprocessing started on the second day when Level-0 (L0) GPS tracking data of each Sentinel-1 satellite are available (the first day is excluded due to the large gap of L0 data occurring on both satellites). For Sentinel-1A, it starts on 7th April 2014 whereas, for Sentinel-1B, it begins on 28th April 2016. Thus, the reprocessing campaign covers 2461 and 1709 days for Sentinel-1A and Sentinel-1B, respectively. From this amount of days, there are four days for Sentinel-1A (i.e., 30th and 31st May, 1st June and 6th July 2014) and six days for Sentinel-1B (i.e., 10th, 11th, 12th, 22nd and 31st May and 5th June 2016) missing, because no L0 data was available for these days. GPS data from the two satellites are routinely made available in RINEX (Receiver INdependent EXchange, Romero, 2020) format 3.03 by the CPOD Service on the ESA COAH.

The GPS receivers (Zangerl et al., 2014) provide observations with 10 s time interval, but the epochs are generally not at 0, 10, 20..., seconds but, for example, at 7, 17, 27..., seconds. This typically changes at every receiver reboot (see Table A1 of the appendix). These reboots have occurred more often for Sentinel-1A.

Sentinel-1A had a short interval in 2015 (between end July until mid-September) where the redundant receiver was partly running instead of the main receiver. Sentinel-1B has always been running on the main receiver.

Satellite attitude is either modelled according to the attitude law (Peter et al., 2017; Miranda, 2015) or attitude quaternions provided by the CPOD Service (also available from the ESA COAH) are used. The latter are based on quaternions provided by the satellite Attitude and Orbit Control System (AOCS) and filled with modelled attitude when measured quaternions are missing. The nominal Sentinel-1 attitude consists of two rotations. The first one is the rotation from J2000 to ZDORF (Zero-Doppler Orbital Reference Frame, Fiedler et al., 2005) and the second one, also called roll steering law is the rotation from ZDORF to satellite-body fixed system (Miranda, 2015). The attitude law causes the satellites always flying with the satellite body tilted to the right and the solar panels are always fixed in a 30° tilt w.r.t. to the satellite body (see Fig. 1). Information about centre of mass coordinates, mass history, GPS ARP coordinates, and manoeuvre history is available via the Sentinel Online web pages[3]. An ANTEX (ANTenna EXchange, Rothacher and Schmid, 2010) file for the antenna PCOs and PCVs (Phase Centre Variations) is also available through this website. It should be noted that the ARP coordinates are different to those listed in Peter et al., 2017. The antenna PCOs and PCVs are also different to those used in Peter et al., 2017 and Peter et al., 2020a. Antenna PCOs and PCVs are derived from an off-line reprocessing reported in Fernández et al., 2019. Both the ARP and PCO values currently used by the CPOD Service (and also used by all centres and for the entire period of time of this reprocessing) can be found in Table 1.

3. POD processing strategy

Orbit determination strategies used by the CPOD Service and the other centres are based on a reduced-dynamic approach (Wu et al., 1991). The methods mainly differ in the selection of different background models (e.g., gravity field model), if and how gravitational forces are modelled, and in the number of empirical parameters used. Table 2 lists the different processing set-ups of the centres (GMV, 2021).

[3] https://sentinels.copernicus.eu/web/sentinel/technical-guides/sentinel-1-sar/pod.

Table 2
POD processing parameters and models used by each centre.

Parameter/Model		Analysis centre				
		AIUB	CPOD	DLR	TUD	TUM
Software	Name and version	Bernese GNSS Software v5.3 (Dach et al., 2015)	NAPEOS (Springer et al., 2011)	GHOST 2276 (Wermuth et al., 2010)	GIPSY-X v1.5 (Bertiger et al., 2020)	Bernese GNSS Software v5.3 (mod)
Arc cut	Arc lengths	24 h	32 h	30 h	30 h	30 h
	Handling of manoeuvres	No, days are not processed	Considered and calibrated	Considered and calibrated	Considered and calibrated	No, days are not processed
	Handling of data gaps	No	Yes	Yes	Yes	No
Reference system	Polar motion and UT1	CODE final products	IERS finals2000A.data	igs96p02.erp	JPL Final products	IERS finals2000A.data
	Pole model	IERS 2010 Conventions (Petit and Luzum, 2010)	IERS 2010 Conventions	None	IERS 2010 Conventions	IERS 2010 Conventions
	Precession/Nutation	IERS 2010 Conventions	IERS 2010 Conventions	IERS 2010 Conventions	IERS 2010 Conventions	IERS 2010 Conventions
Satellite reference	Attitude model	Nominal attitude law	Quaternions	Nominal attitude law	Quaternions	Nominal attitude law
Gravity	Gravity field (static)	GOCO05s (120 × 120) (Pail et al.,2010)	EIGEN.GRGS.RL04 TVG (120 × 120) (Lemoine et al., 2019)	GOCO03S (100 × 100) (Pail et al.,2010)	EIGEN.GRGS.RL04. MEAN-FIELD with quadratic_mean_pole (200 × 200)	EIGEN GL04C (120 × 120) (Förste et al., 2006)
	Gravity field (time varying)	IERS 2010 Conventions	Drift/annual/semi-annual piece wise linear terms up to degree/order 90	None	Drift/annual/semi-annual piece wise linear terms up to degree/order 90	Drift of 20, 30, 40
	Solid Earth tides	Applied (IERS 2010)	Applied (IERS 2010)	Applied	Applied (IERS 2010)	Applied (IERS 2010)
	Ocean tides	EOT11A (50 × 50) (Savcenko et al., 2012)	FES2014 (100 × 100, 142 tidal constituents) (Lyard et al., 2021)	Applied (FES 2004) (Lyard et al., 2006)	Applied (FES2004)	FES2004 (50 × 50)
	Atmospheric gravity	None	AOD1B RL06 (100 × 100) (Dobslaw et al., 2018)	None	AOD1B RL06 (180 × 180)	None
	Atmospheric tides	None	AOD1B RL06 (100 × 100)	None	None	None
	Earth pole tide	IERS 2010	IERS 2010	None	IERS 2010	IERS 2010
	Ocean pole tide	IERS 2010	IERS 2010	None	IERS 2010	IERS 2010
	Third bodies	Sun, Moon, Planets DE405 (Standish, 1998)	Sun, Moon, Planets DE421 (Folkner et al., 2009)	Sun, Moon (analytical series)	Sun, Moon, Planets (IERS 2010)	Sun, Moon, Planets DE405

Surface forces and empirical parameters	Radiation pressure model	None	Box-wing model (with re-radiation)	Box-wing model (with re-radiation)	Box-wing model	Box-wing model (with re-radiation)
	Earth radiation	None	Albedo and Infra-red applied	None	Albedo and Infra-red applied	Albedo and Infra-red applied
	Atmospheric density model	None	NRLMSISE-00 (Picone et al., 2002)	NRLMSISE-00	DTM2000 (Bruinsma et al., 2003)	MSISE-90 (Hedin, 1991)
	Radiation pressure coefficient	None	Fixed to 1.0	1/arc (estimated)	1/arc (estimated)	1/arc (estimated)
	Drag coefficients	None	1/arc (estimated)	1/arc (estimated)	1/arc (estimated)	1/arc (estimated)
	1/rev empiricals	None	16 sets/arc in along- and cross-track (constant/ sine/cosine)	None	In along- and cross-track (sine/cosine)	2 sets/arc in along- and cross-track direction (sine/cosine)
	Other empiricals	Constant empirical accelerations in RTN every 6 min (constrained)	None	Constant empirical accelerations in RTN every 10 min (constrained to zero)	Constant empirical accelerations in RTN every 10 min (daily biases removed)	Stoch. velocity changes every 15 min
GPS measurements	Relativity	Applied	Applied (IERS 2010)	Applied	Applied	Applied
	Sampling	10 s	10 s	30 s	30 s	10 s
	Observations	Iono-free linear combination of phase measurements (pseudo-range: clock synchronisation and Melbourne-Wübbena linear combination)	Iono-free linear combinations of phase and pseudo-range measurements	Iono-free linear combinations of phase and pseudo-range measurements	Iono-free linear combinations of phase and pseudo-range measurements	Iono-free linear combinations of phase and pseudo-range measurements
	Observation sigma (pseudo-range/carrier phase)	None	0.8 m / 10 mm	1.0 m / 10 mm	1.0 m / 10 mm	1.0 m / 10 mm
	Antenna PCO/PCV	Applied (AIUB maps)	Applied (CPOD maps1)	Applied (CPOD maps1)	Applied (CPOD maps1)	Applied (CPOD maps1)
GPS parameters	Receiver clocks	Per epoch, every 10 s	Per epoch, every 10 s	Per epoch, every 10 s	Per epoch, every 30 s	Per epoch, every 10 s
	Receiver ambiguities	Estimated (fixed)	Estimated (fixed)	Estimated (fixed)	Estimated (fixed)	Estimated (fixed)
	Fixed GPS orbits & clocks (sampling, biases (yes/no))	CODE repro/final products[2] (5 s, yes)	CODE repro/final products[3] (5 s, yes)	CODE repro/final products[3] (5 s, yes)	JPL Final / IGS14 (30 s, yes)	CODE repro/final products[2] (5 s, yes)

[1] The CPOD PCO/PCV maps are available in ANTEX format at https://sentinels.copernicus.eu/web/sentinel/technical-guides/sentinel-1-sar/pod/satellite-parameters.
[2] The CODE repro products (Villiger et al., 2020) have been used for the interval of time between the start of the mission until 31/12/2018, whereas the CODE final products have been used on 2019/2020.
[3] The CODE repro products have been used for the interval of time between the start of the mission until 31/12/2019, whereas the CODE final products have been used on 2020. The CODE final products have also been used on mid-2019 from 9th June to 7th September due to a problem with the reprocessed products.
Note: RTN (Radial, Transverse and Normal).

One of the main differences between the centres is that different software packages are used. The arc length of the processed solutions is varying between 24 h and 32 h. TUD is not using CODE GPS products but corresponding products from JPL. Other differences to be highlighted are: (a) AIUB compensates the non-gravitational forces with empirical parameters, so-called piece-wise constant accelerations, with a short duration of only six minutes in all three orbit frame directions whereas the other centres model the non-gravitational forces and add more (DLR, TUD, TUM) or less (CPOD) empirical parameters, and (b) AIUB applied their own estimated PCV maps in their processing whereas all other centres made use of the PCV maps provided by the CPOD Service.

Such differences in the processing set-ups of the centres are welcome for the reprocessing because a certain diversity is good to minimise the possibility of common errors. The AIUB solution, with its full empirical modelling of the non-gravitational forces, is particularly important to discover remaining problems in the non-gravitational force modelling and in the satellite geometry (ARP, PCO and centre of mass) as already reported in Peter et al., 2017.

4. Analysis of results

The analysis of results is divided into four subsections. First, an analysis of all solutions generated by each centre is performed. This analysis includes processing metrics and estimated parameters calculated during the processing of the orbit solutions. Orbit overlaps are also evaluated. Second, some results of the combined orbit solution generated from all available solutions are given. Third, the orbit comparisons calculated between each orbit solution against the combined solution are addressed. Finally, an analysis of a particle impact on Sentinel-1A satellite on 23rd August 2016 is shown.

4.1. Pre-analysis of the provided solutions

The study of the orbit solutions provided by each centre focuses on the GPS observation residuals and estimated parameters obtained during the processing of their orbit solutions. This study also addresses the orbit overlaps calculated from consecutive solutions of each centre. The outcome of these parameters, despite not being definitive to evaluate the final quality of the orbit solutions, may allow us to predict possible degradations on the orbit solutions generated. Moreover, the analysis of these parameters may be used to identify possible improvements to be done on, for example, the orbit modelling used during the processing.

Two of the centres (AIUB and TUM) have not provided orbit solutions for days with either manoeuvres or large gaps of L0 data. Each of the Sentinel-1 satellites is manoeuvred about once per week to stay in a pre-defined orbit tube (GMES, 2010; Martin Serrano et al., 2012). This is necessary to guarantee the 12-day repeat cycle of the observations. Thus, the data contribution of these two centres represents 80–85 % (for Sentinel-1A) and 85–90 % (for Sentinel-1B) of the orbit solutions provided by any of the other three centres (CPOD, DLR and TUD).

4.1.1. GPS observation residuals

The comparison of GPS pseudo-range and carrier phase residuals from different processing centres is not straight forward. Different software packages were used for the processing. In addition, different processing strategies, orbit parametrisations and observation editing strategies lead to different results, which might not be directly comparable.

Fig. 3 depicts the daily RMS of the pseudo-range residuals obtained by each centre (in the case of AIUB, these are the pseudo-range residuals from the clock synchronisation step before the actual orbit determination). The image on the left shows the results for Sentinel-1A and the image on the right presents the outcome for Sentinel-1B. Similar pattern and values are achieved by all solutions over time, except for TUD residuals, which show lower values as a result of code smoothing in their processing. Despite this fact, the pseudo-range residuals are almost consistent over the whole period of time evaluated. Periods of time with small (e.g., April 2018) or large (e.g., from January 2017 to February 2020) ups and downs may be directly related to flex power operations carried out on GPS satellites (Steigenberger et al., 2019).

The outcome on the daily RMS carrier phase residuals is displayed in Fig. 4. Significant differences between centres are visible. Similar patterns and even values can be observed for AIUB, CPOD and DLR solutions. The three centres were using the same GPS products from CODE. A feature of these solutions is the sinusoidal pattern of the obtained carrier phase residuals, which is not visible on solutions that make use of other GPS products (i.e., TUD). TUD provide more consistent residuals over time,

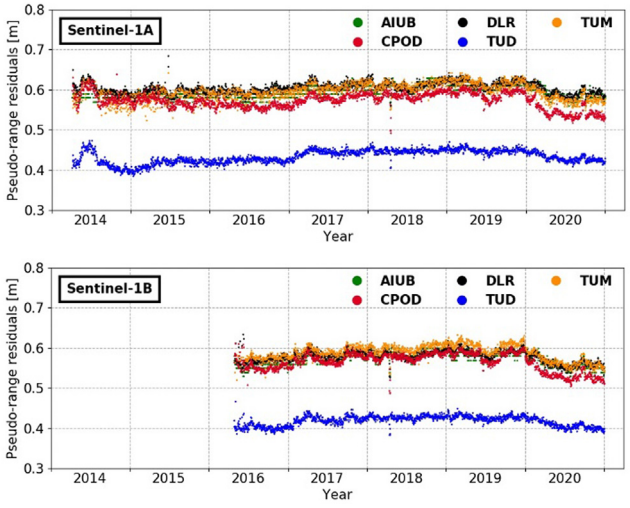

Fig. 3. Pseudo-range residuals [daily RMS, m] achieved by all centres over time for Sentinel-1A (top) and Sentinel-1B (bottom).

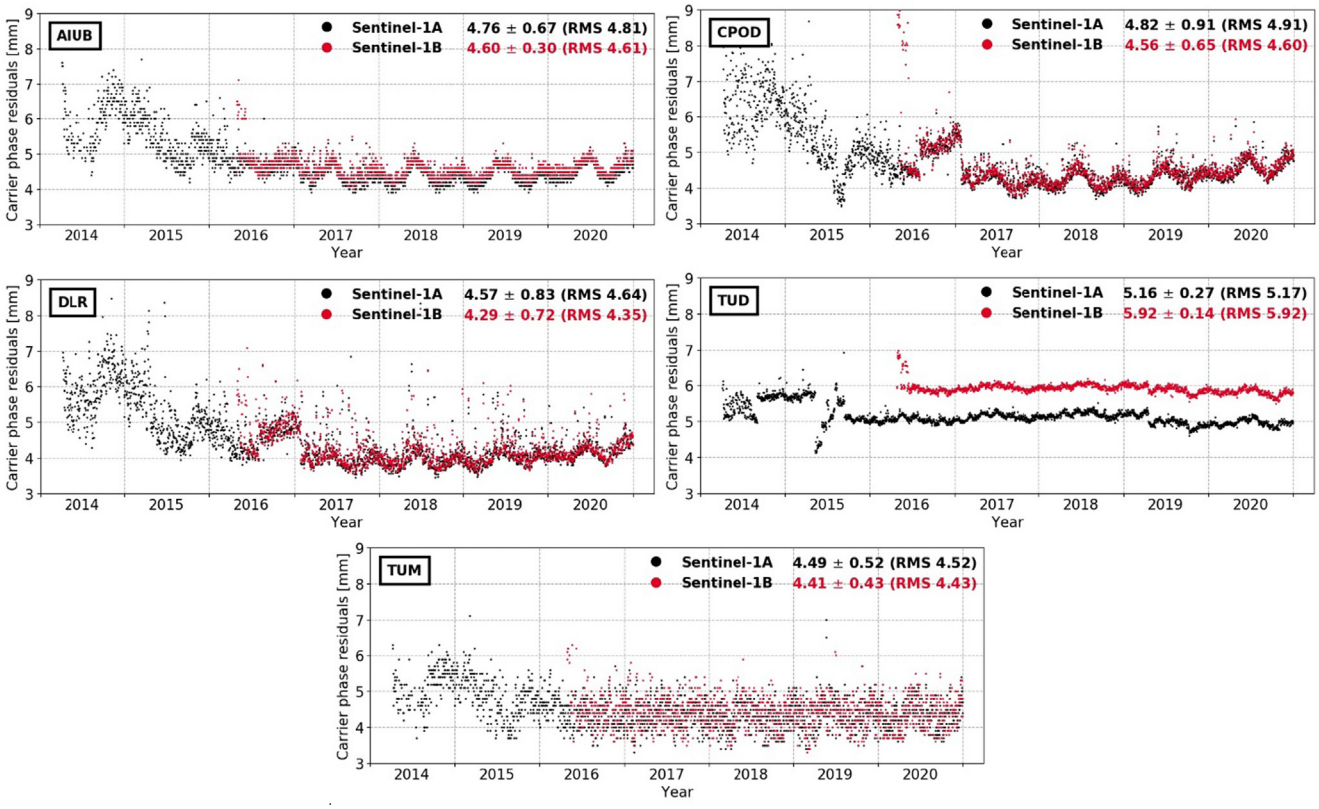

Fig. 4. Carrier phase residuals [daily RMS, mm] achieved by each solution over time. One plot per centre showing the results for both Sentinel-1 satellites. Mean ± STD (RMS) statistics are in mm.

but with higher RMS values. The differences between TUD solutions for the two different satellites are due to the different observation epochs of Sentinel-1A and Sentinel-1B (see Table A1). The GIPSY-X software does not interpolate the 30 s GPS clocks. Therefore, this leads to different clock interpolation errors mapping into the carrier phase residuals.

In general, the pattern shown on the carrier phase residuals of each solution remains stable for the whole period of time evaluated, except for years 2014 and 2015. During these years, the solar activity has been higher than in more recent years. The impact of this on the carrier phase residuals of the GPS receiver data has already been shown in van den IJssel et al., 2016 for the Swarm satellites (carrying the same type of receiver as Sentinel-1 satellites). Fig. 5 shows the RMS errors of the Sentinel-1A carrier phase residuals of CPOD solution for December 2014 (left) and December 2018 (right) in a geographical distribution. The increased RMS errors in the polar regions in December 2014 are clearly visible. This increased RMS is caused by receiver tracking problems during times with high solar activity (van den IJssel et al., 2016).

As seen in Fig. 4, the residuals obtained by CPOD and DLR solutions show a jump during the second half of year 2016 and the very beginning of year 2017, not seen on AIUB and TUM solutions (also using CODE products). AIUB orbits are most reduced-dynamic. The empirical parameters used by this solution might absorb weird effects seen in the residuals on the other solutions. On the other hand, the noisier results observed on the carrier phase residuals from TUM can be related to a very stringent outlier detection used by this centre.

Fig. 6 aims to highlight the differences on the Sentinel-1A carrier phase residuals obtained from the previous operational orbit solution generated by the CPOD Service and the current reprocessed one (Sentinel-1B shows the same pattern). The same figure for pseudo-range residuals is not shown because the updates did not have a significant impact on these residuals.

The main causes for the lower carrier phase residuals in the reprocessed CPOD solution are: (a) the use of 5 s GPS clocks instead of 30 s, (b) the update of the orbit parametrisation with more empirical parameters than before, (c) the correction of the ARP coordinates and, (d) the PCO update. The increase of the carrier phase residuals occurring during the second-half of year 2020 for the former operational CPOD solution was due to the switch to carrier phase ambiguity fixing but not yet using 5 s GPS clocks for the processing. When switching to 5 s GPS clocks in early 2021 (not shown in the plot), the carrier phase residuals of the operational solution also dropped down to the level of the reprocessed orbit series.

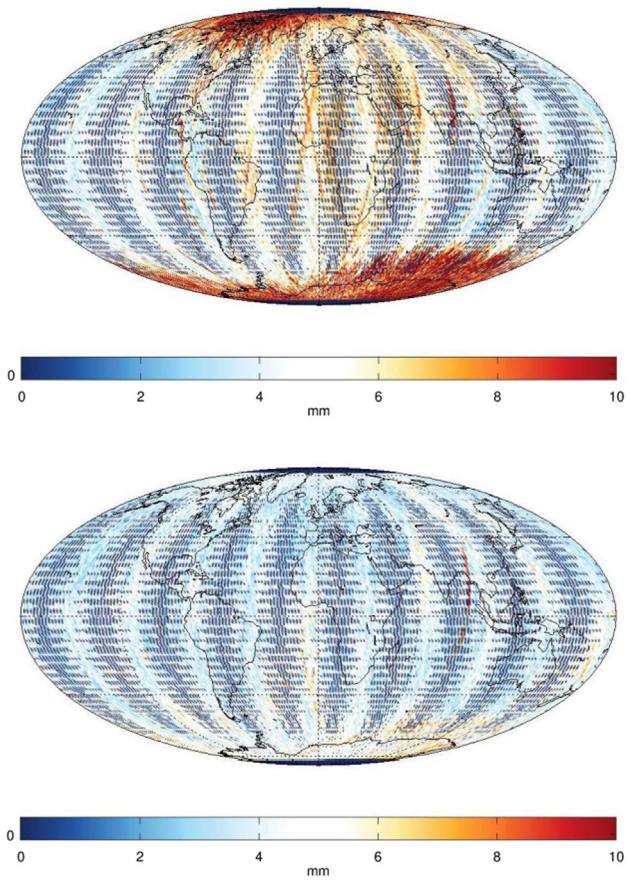

Fig. 5. Geographical distribution of RMS errors of Sentinel-1A carrier phase residuals of CPOD orbit solution (top December 2014, and bottom December 2018). A very few outliers have been removed.

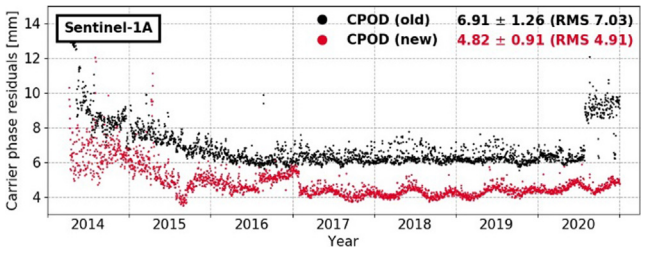

Fig. 6. Carrier phase residuals [daily RMS, mm] achieved by the former CPOD solution and the new reprocessed CPOD solution over mission time of the Sentinel-1A satellite. Mean ± STD (RMS) statistics are in mm.

4.1.2. Estimated parameters

Direct comparisons between the estimated parameters of all centres is also not straight forward due to the variety of the parameters used by each of them (see Table 2). Thus, the analysis of the estimated parameters has been restricted to the CPOD solution being the official reprocessed orbit solution. The parameters estimated for the CPOD solutions are 16 sets of CPR parameters in along- and cross-track directions (each set is 2 h long), and one drag scale factor. The CPOD solution does not estimate a radiation pressure coefficient (C_r) as other centres do, but its value is fixed to 1.0. This value is the result of a long-term estimation of radiation pressure coefficients for all Sentinel-1, -2, and -3 satellites (Peter et al., 2020c). The C_r estimates for the two Sentinel-1 satellites still showed seasonal variations, which are not yet fully understood, but with 1.01 the mean C_r values were very close to 1.0 for both satellites.

The 16 sets of each CPR parameter are averaged to one daily mean to ease the analysis. The evolution of this daily mean is depicted in Fig. 7 and presented in different panels (per satellite and local orbit direction). The parameters show repeatable systematics over the year. The eclipse period between May and August each year clearly leads to significant variations in all parameters. For the rest of the year the parameters are close to zero. Exception is the constant cross-track parameter, which shows a significant constant bias of 12.41 nm/s^2 and 12.51 nm/s^2 for Sentinel-1A and Sentinel-1B, respectively. Sentinel-1 satellites have a complex body and this implies difficulties to set-up a precise macro model for them. Accounting for self-shadowing effects (Peter et al., 2020a) can improve the non-gravitational force modelling, but the systematics and the cross-track bias cannot be fully removed. The cross-track biases might be related to a still remaining offset in the antenna cross-track (Y) direction. Future work will, therefore, be focussed on the further improvement of the satellite macro model and the removal of this bias.

Fig. 8 shows the daily evolution of the estimated drag scale factor of the CPOD solution over time. Similar to the case of the CPRs, the estimated values of the drag combine periods of time where high consistency is achieved (with values between 0.5 and 0.8) and periods of time where this consistency is broken (falling down and even obtaining negative values). As the CPRs case, these consistency breaks also occur during eclipse periods of Sentinel-1 satellites. Negative values for the drag scale factor have no physical meaning, but the drag scale factor and the CPR along-track constant parameter are correlated to some extent, which is part of the reason for such non-physical estimates. This might be minimised by adding stronger constraint to the drag scale factor. The drag scale factor estimates confirm that eclipse periods have a clear impact on the estimation of parameters for the Sentinel-1 CPOD solutions. More studies have to be performed to mitigate this effect. The evolution of the beta angle (i.e., the angle between the satellite orbit plane and the vector to the sun) has also been included in Fig. 8 in order to indicate the incidence of eclipse periods on Sentinel-1 satellite orbits.

4.1.3. Overlaps

The orbit overlaps between consecutive solutions of each centre have been calculated only considering the midnight epoch. Longer orbit overlap analysis has not been possible because AIUB has delivered only 24 h solutions. To avoid harming the final statistics, a few outliers have been filtered out from the final outcome. Table A2 in the appendix summarises the complete list of the removed orbit

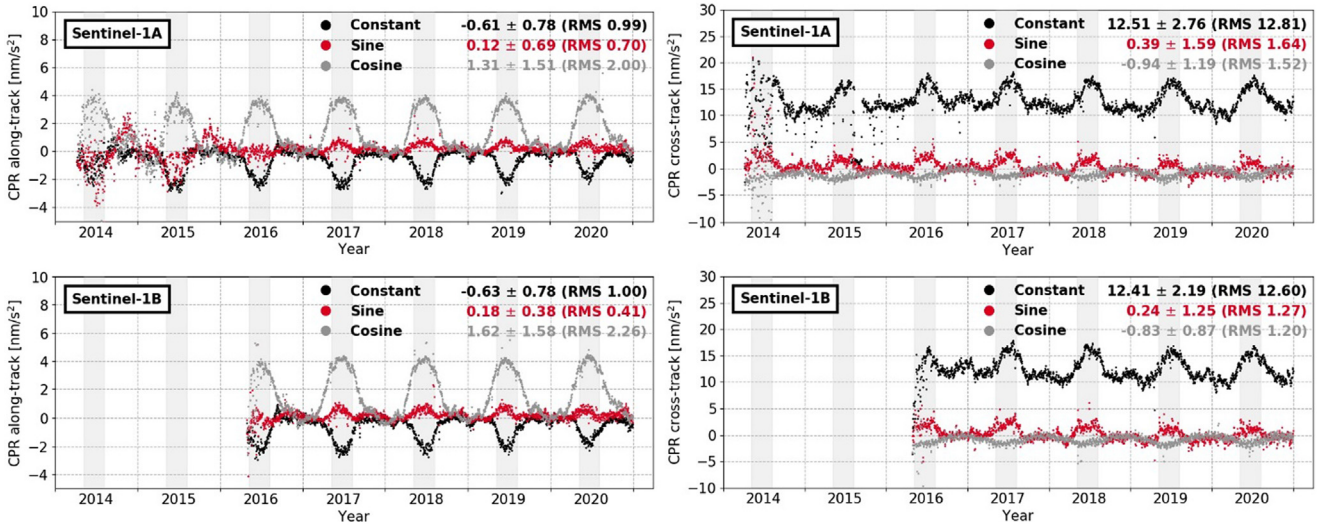

Fig. 7. Estimated CPR parameters [daily mean, nm/s^2] of the CPOD solution over time. The results are shown per satellite (top Sentinel-1A and bottom Sentinel-1B) and local orbit direction (left along-track and right cross-track). Mean ± STD (RMS) statistics are in nm/s^2. Grey shaded areas correspond to eclipse periods.

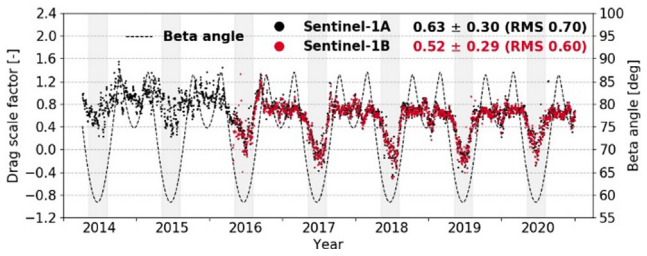

Fig. 8. Estimated drag scale factor [-] of the CPOD solution over time for both Sentinel-1 satellites. Beta angle [deg] is also represented, which values are aligned to drag pattern. Mean ± STD (RMS) statistics refer to drag scale values [-]. Grey shaded areas correspond to eclipse periods.

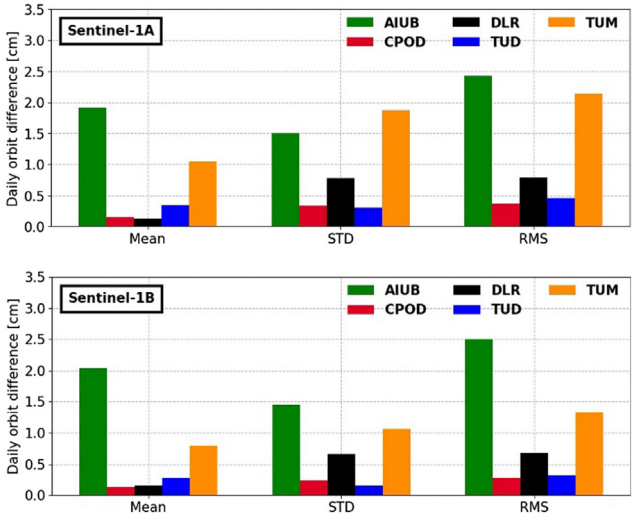

Fig. 9. Statistics of mean, STD and RMS [cm] of the 3D orbit overlaps at midnight epochs for the entire period of time evaluated (top Sentinel-1A and bottom Sentinel-1B).

overlaps, which are mostly the result of large gaps of L0 data occurring between days. Thus, side effects related to orbit estimation will be removed as much as possible from the data shown henceforth.

Fig. 9 shows the mean, STD and RMS for all daily orbit differences found at midnight epochs. Most of the solutions present overlaps with low mean and STD (below 0.5 cm) showing good agreement between consecutive generated orbit solutions. The analysis of the figure also reveals higher statistical measures for AIUB solution, which is due to the shortest processing arc of 24 h. This affects the orbit quality on the arc boundaries. The overlap results from TUM solution also show higher values, which are mainly due to non-zero mean values of the individual components (figures not shown) of the overlap. This non-zero mean values are also present in AIUB overlaps. For the remaining centres, the mean values are close to zero.

In Fig. 10, one example of a temporal evolution of the orbit overlaps for Sentinel-1A is shown. Both the orbit overlaps of the former operational (old) and the reprocessed (new) CPOD solutions are depicted. The significant improvement of the new with respect to the old CPOD solutions is clearly visible. Same result is achieved for Sentinel-1B.

The analysis of the processing metrics, estimated parameters and orbit overlaps of the different solutions shows the variety of topics to be addressed in such a long reprocessing. Systematic effects are visible in all solutions related to (a) the GPS products used, (b) the processing software used, (c) the orbit parametrisation, and (d) the observation handling. It shows how different individual solutions are derived and how difficult an interpretation of the results is. Despite the differences seen here, Section 4.3 shows that a very good consistency is achieved between all solutions.

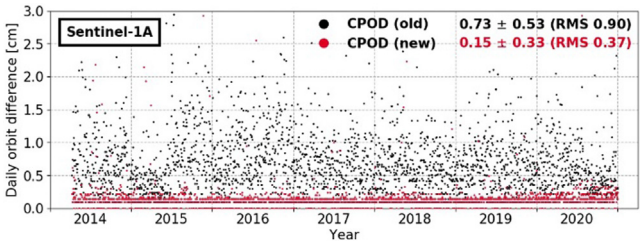

Fig. 10. Orbit overlaps [daily orbit difference, cm] calculated from CPOD solutions (former operational, old, and reprocessed, new) over time for Sentinel-1A. Mean ± STD (RMS) statistics are in cm.

4.2. Generation of the combined orbit solution

As an extra means of being able to compare the different orbit solutions, a combined orbit solution has been generated. This solution is a weighted mean of all solutions used during the combination. This combination follows a similar approach used by the IGS when generating their final solutions (Beutler et al., 1995). Alternative combination schemes have been studied by, e.g., Kobel et al., 2019 for Sentinel-3A.

Each state vector (SV) of the combined solution, $\mathbf{SV}_{\text{comb}}$, which includes position, $\mathbf{r}(t)$, and velocity, $\mathbf{v}(t)$, of the satellite at time t (i.e., $\mathbf{SV}_{\text{comb}}(t) = [\mathbf{r}(t)\mathbf{v}(t)]^{\text{T}}$), is calculated by averaging the SVs of the different solutions to be combined, $\mathbf{SV}_j$, as follows:

$$\mathbf{SV}_{\text{comb}}(t) = \frac{\sum_j \mathbf{SV}_j(t)/w_j}{\sum_j 1/w_j}$$

where $1/w_j$ denotes the weight associated to each orbit solution j on a particular day. These weights are a measurement of the (inverse) distance between the orbits of each centre and the simple arithmetic mean combination (i.e., a priori combined solution setting $1/w_j = 1$).

Let d_j be the modulus of the distance between the position of the a priori combined solution, $\mathbf{r}_0$, and the position of the solution of centre j, $\mathbf{r}_j$, at time t. This is.

$$d_j(t) = \left|\mathbf{r}_0(t) - \mathbf{r}_j(t)\right|$$

If $\mathbf{d}_j$ is the vector built from all distances d_j calculated at every time t of the temporal discretisation (defined by the combination step, which value can be selected by the user) of the desired combined orbit solution, a value $\bar{w}_j$ can be defined as the median of vector $\mathbf{d}_j$. This value $\bar{w}_j$ is scaled by a factor, sc, to obtain the value w_j as $w_j = \bar{w}_j/sc$. The scaling factor is no more than taking the maximum value $\bar{w}_j$ achieved by any of the centres j participating to the combination, i.e.

$$sc = \max\{\bar{w}_1, \bar{w}_2, \cdots, \bar{w}_j, \cdots\}$$

Therefore, the desired weight, $1/w_j$, corresponding to a particular day of centre j can be finally obtained.

Although the desired approach is to use all available orbit solutions for the combination, there is a limitation on the current tool performing such task. If one of the solutions to be combined presents a data gap (mostly as a result of being processed from a large gap of L0 data), the combined solution will be generated with such gap regardless of whether the rest of solutions are complete. To avoid this fact, incomplete solutions (i.e., not fulfilling the 24 h length of the day) provided by any centre are not used for the combination (see complete list in Table A3 of the appendix). Moreover, a priori cross-comparison analysis performed between all solutions has shown that a few orbit solutions present noticeable differences with respect to the others on a few specific days. As a measure to prevent a bad combination from the use of any of them, these solutions have also been excluded from the combination. A complete list of these solutions including the reason for exclusion is summarised in Table A3. It must be remarked that, despite being removed from the combination, all solutions have been used to calculate the orbit comparisons against the resulting combined solution unless otherwise stated.

The resulting statistics of the orbit solutions used during the combination is shown in Fig. 11. The figure presents percentages and total number of solutions to generate the combined solution for the entire period of time evaluated (see table attached to the figure). On the vast majority of the cases, the combining tool has made use of all solutions. Only on a very few cases (23 for Sentinel-1A and 14 for Sentinel-1B), the combined solution has been generated by one (only CPOD) or two solutions (CPOD plus another). When only two solutions are combined, the algorithm gives the same weight to both solutions. Thus, the resulting combined solution could be severely impacted if one of these combined solutions is significantly degraded. The total percentage when using 4 and 5 solutions for the

Total number (%)	
Sentinel-1A	**Sentinel-1B**
4 (0.16 %)	3 (0.18 %)
19 (0.77 %)	11 (0.65 %)
389 (15.83 %)	226 (13.27 %)
31 (1.26 %)	6 (0.35 %)
2014 (81.97 %)	1457 (85.55 %)

Fig. 11. Number and percentage of orbit solutions used to generate the combined orbit solution for Sentinel-1A and Sentinel-1B satellites.

combination is in line with the total amount of solutions available (see Section 2).

The results of how the combination has worked can be retrieved from the values of the weights the combining tool has given to each solution and day. An example of these values over time for two of the centres may be observed in Fig. 12. The weights of TUD and TUM solutions are depicted for both Sentinel-1 satellites. It must be noted that a higher value on the weight implies a higher contribution of the solution to the combined solution. Considering this, TUD (as well as CPOD and DLR solutions) is one of the centres contributing relatively much to the combined orbit. It can be seen in the figure that the main line is around a value of 0.2. The rest of points near 0.4 or above are due to days with either manoeuvres or gaps of L0 data where a few orbit solutions (usually CPOD, DLR and TUD) are available for the combination. On the other hand, the weights obtained for TUM solution are a little bit lower than the ones obtained by TUD (~0.17 on average). From this curve of points, it can be observed that TUM solution is somehow affected by the periods of time where satellite eclipses occur (between May and August each year). The combining tool gives lower values to TUM solution on such days.

A summary of the outcome on the weight values can be found in Fig. 13, where the mean of the daily weight values given to each solution is shown (left panel). From this figure, it can be seen that CPOD, DLR and TUD are the solutions most contributing and practically with similar weight values to the generation of the combined orbit solution. If only days where all 5 solutions are used (right panel) when neither manoeuvres nor gaps of L0 data occur, similar values are obtained with a slight decrease in the results of CPOD and TUD solutions.

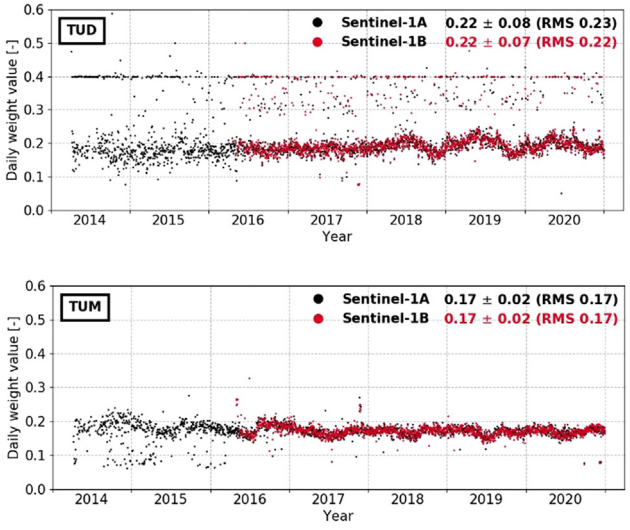

Fig. 12. Daily weight values [-] given to TUD (top) and TUM (bottom) solutions over time for the generation of the combined orbit solution. Mean ± STD (RMS) statistics are also shown [-].

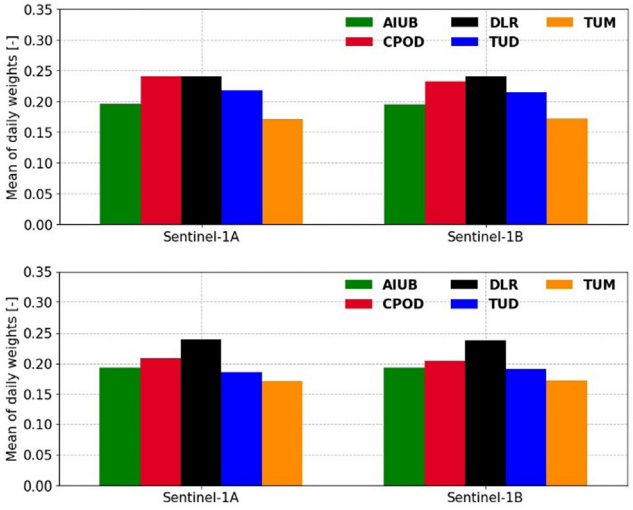

Fig. 13. Mean of daily weight values [–] given to all centres for the generation of the combined orbit solution (top: all days; bottom: days with 6 solutions on the combination).

A weak point of this combination algorithm is that the weights given for the individual solutions cannot be interpreted as a direct quality measure for the solutions. The majority of solutions fitting best to each other will get the largest weights without being able to judge which solution is better or worse. Without having an independent observation technique available for external validation, this problem cannot be overcome. Nevertheless, Kobel et al., 2019 showed for Sentinel-3A that weights derived from a Variance Component Estimation (VCE) correspond to the ranking of the individual solutions in an independent SLR validation. The combination algorithm used here is different to a VCE approach, but the resulting ranking of the solutions is equivalent in most cases. In any case, the combined orbit based on weighted average at least gives the possibility to assess the consistency of various orbit solutions.

As done for the solutions of all centres, the orbit overlaps for the combined orbit solution have also been calculated. Fig. 14 depicts the temporal evolution of the orbit differences at midnight epochs for the entire period of time evaluated and for both Sentinel-1 satellites. The same days listed in Table A2 and affecting the orbit overlaps of two or more solutions have been filtered out from the outcome of the orbit overlaps of the combined solution. As commented before, these filtered-out days contain large gaps of L0 data at the beginning or end of the day. Noticeable differences between solutions are found when large gaps of L0 data occur, and therefore, the resulting combined orbit is directly impacted by such differences. These orbit overlaps have consequently been removed from the outcome shown in the figure.

The results on the orbit overlaps display a mean value below 0.5 cm for both satellites with a standard deviation near 0.4 cm for Sentinel-1A and near 0.3 cm for Sentinel-

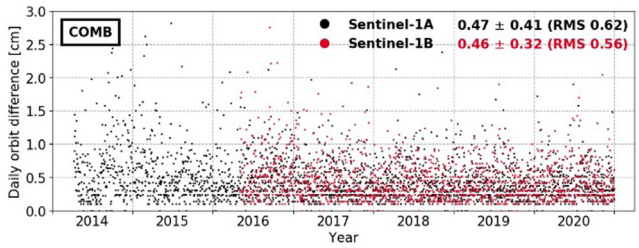

Fig. 14. Orbit overlaps [daily orbit difference, cm] calculated for the combined orbit solution over time for Sentinel-1A and Sentinel-1B satellites. Mean ± STD (RMS) statistics are in cm.

1B. This small difference on the standard deviation values between satellites can be directly related to the values achieved by Sentinel-1A during years 2014 and 2015, which are more disperse. Despite this fact, the orbit overlaps of the combined orbit solution present a very good performance.

4.3. Orbit comparisons

The analysis of the results continues by showing the outcome from the calculated orbit comparisons of all solutions provided by the different centres against the generated combined orbit solution from previous section. Periods of time with manoeuvres or data gaps have been filtered out from each daily comparison performed with a safe margin of 5 min before and after the occurrence of the event. Thus, the following results can be considered fair for all solutions involved regardless if one centre has provided solutions on days with manoeuvres and/or gaps of L0 data or not. Moreover, three daily orbit comparisons from Sentinel-1A AIUB solution have also been removed due to the switch on the GPS receiver from nominal to redundant or vice versa (i.e., on 28th July, 3rdAugust and 14th September 2015).

Fig. 15 depicts the temporal evolution of these orbit comparisons for Sentinel-1A and Sentinel-1B satellites. The figure precisely shows the daily 3D RMS obtained for each solution (if available) separately to better identify any peculiar pattern. Each panel of the figure also contains the results for both satellites together in order to show inconsistencies between satellites if any.

From the analysis of the figure, it can be said that: (a) the vast majority of the comparisons for all centres are well below 1 cm [3D RMS]; (b) most of the Sentinel-1A comparisons show more dispersion during years 2014 and 2015; (c) CPOD and TUD solutions present the most consistent comparisons, which are closely followed by DLR solution; (d) the comparisons of AIUB and TUM solutions show slightly larger differences to the combined orbit during eclipse periods; (e) the comparisons of the solutions using CODE products show slightly larger differences to the combined orbit during the second half of year 2016 and the very beginning of year 2017 coinciding with the results seen for the carrier phase residuals (the residuals from AIUB solution did not present any weird behaviour because it is absorbed by the empirical parameters; on the contrary, the orbits show the largest differences to the combined orbit); and (f) the Sentinel-1A orbit comparisons are worst when the redundant GPS receiver was running (third quarter of year 2015).

The results show that there is a strong agreement between all solutions while being generated by different software packages. They all vastly fulfil the accuracy requirement of 5 cm [3D RMS] required for the orbit products generated for Sentinel-1 mission. Moreover, some improvement may still be done to the orbit modelling in order to minimise the impact of eclipse periods on the generation of the solutions. The effect of these eclipse periods on the carrier phase residuals and estimated parameters is significant for some of the centres compared to epochs where the satellites are not in eclipse. On the other hand, the time period of the redundant receiver on Sentinel-1A is too short to properly analyse the data with regard to the estimation of the corrected PCO, and to generate a smooth PCV map. The consistency between the various orbit solutions is less good as for the rest of the mission time, but it is still well below the 5 cm requirement.

Finally, Fig. 16 and Fig. 17 show the mean of the daily RMS and daily mean per orbit component, respectively. They confirm the very good consistency between all solutions. The mean of the daily 3D RMS is below or near 0.5 cm for the vast majority of the solutions for both Sentinel-1 satellites.

4.4. 2016 Sentinel-1A particle impact analysis

On 23rd August 2016, a millimetre-size space debris or micrometeoroid hit one of the solar panels of Sentinel-1A satellite causing slight changes in the orientation and the orbit of the satellite[4]. Krag et al., 2017 analyses the event and characterises it providing the mass and size of the particle from attitude and orbit data. From these data, an estimation of the impact vector is also calculated, the particle was moving towards the satellite from the front left of the satellite's direction in a 45° angle, and with a slight angle from the bottom. The exact time of the event was deduced to be at 17:07:37 h (UTC, Coordinated Universal Time).

This section aims to address how a particular event such as a particle impact may be detected from the analysis of the processing metrics, estimated parameters or cross comparisons against other orbit solutions, and how all these parameters take benefit from modelling such event as a manoeuvre. Combined orbit solutions will be generated to support the results.

For the case under study, there have been four centres able to generate an orbit solution on this day: AIUB, CPOD, DLR and TUD. The latter three have

[4] https://www.esa.int/Applications/Observing_the_Earth/Copernicus/Sentinel-1/Copernicus_Sentinel-1A_satellite_hit_by_space_particle.

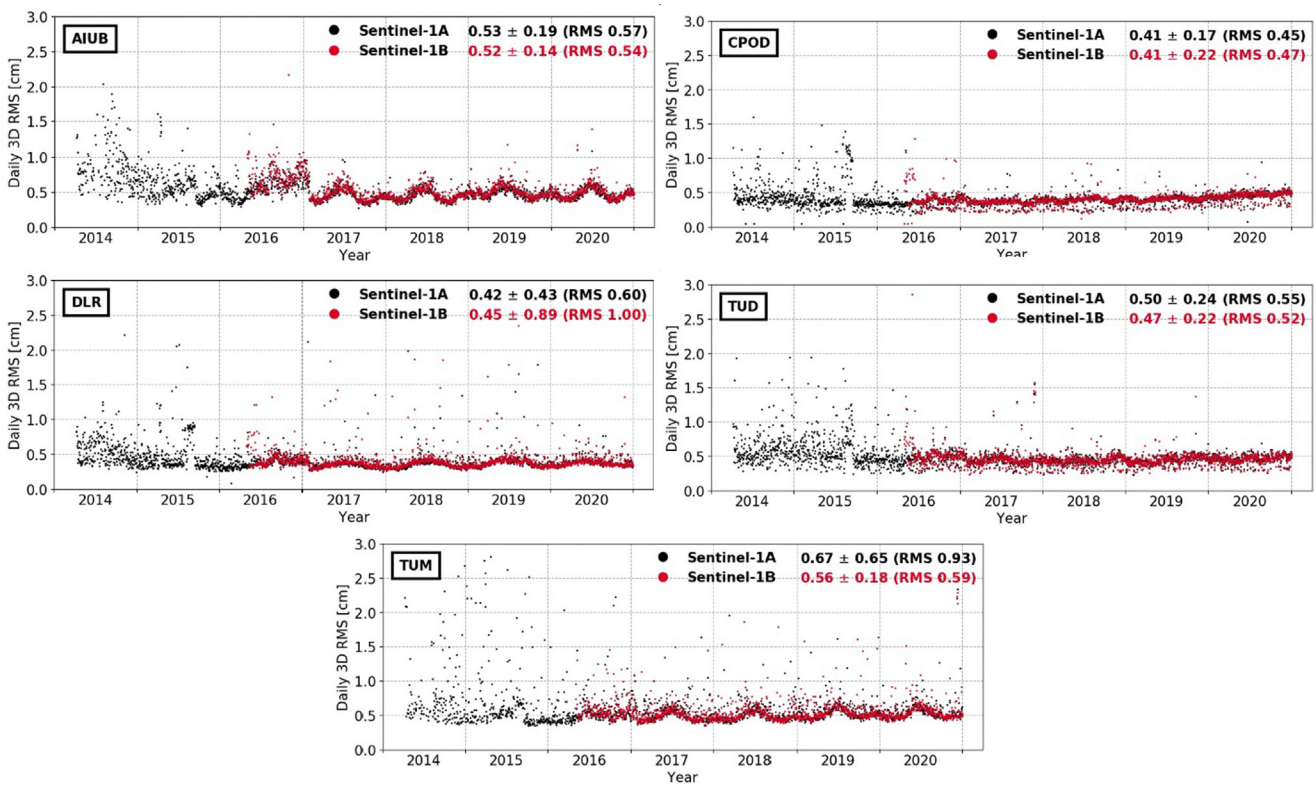

Fig. 15. Orbit comparisons [daily 3D RMS, cm] calculated from each solution against the combined orbit solution. One plot per solution showing the results for both Sentinel-1 satellites. Mean ± STD (RMS) statistics are in cm.

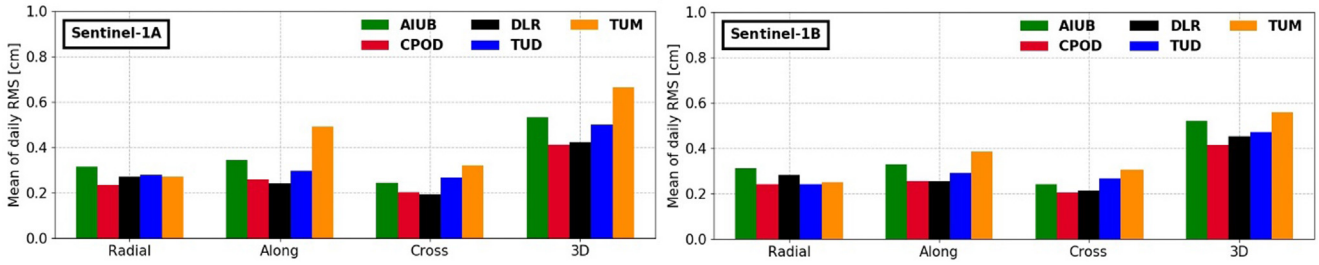

Fig. 16. Mean of daily RMS in radial, along-track, cross-track and 3D [cm] of the orbit comparisons calculated from each solution against the combined orbit solution (left Sentinel-1A and right Sentinel-1B).

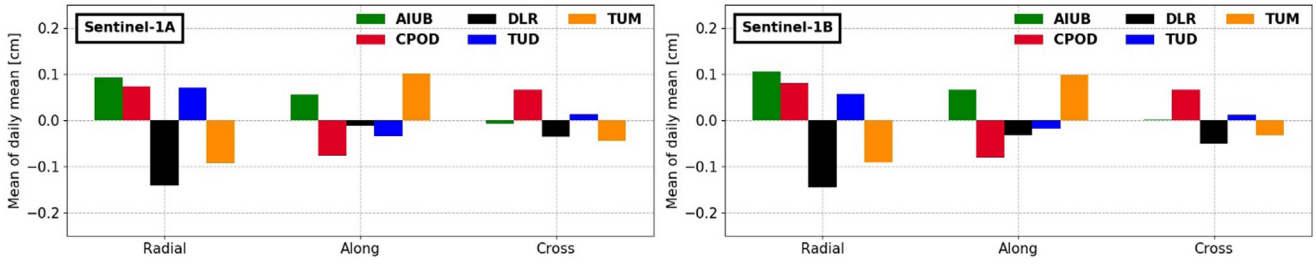

Fig. 17. Mean of the daily radial, along-track, and cross-track mean [cm] of the orbit comparisons calculated from each solution against the combined orbit solution (left Sentinel-1A and right Sentinel-1B).

Table 3
Estimated acceleration values [mm/s^2] in RTN reference frame used by each centre providing solution in order to model the Sentinel-1A particle impact on 23rd August 2016 (manoeuvre of 1 s long).

Centre	Estimated acceleration values [mm/s^2]		
	a_R	a_T	a_N
AIUB	None	None	None
CPOD	−0.117	−0.659	0.695
DLR	−0.087	−0.659	0.667
TUD	−0.109	−0.657	0.679

the ability to estimate manoeuvres. The estimated acceleration values (on the RTN reference frame) calculated by each centre and used to model the particle impact are listed in Table 3. Although the particle impact may be considered instantaneous, it has been modelled by a manoeuvre of 1 s duration. A more reduced time could be used, resulting in an increment of the values given in Table 3. The estimated values should be multiplied by the same proportional value the manoeuvre time is reduced.

From the values in Table 3, the direction of the particle when the impact occurred can be deduced. The particle was moving towards the satellite from the front left of the satellite with an angle between 45° and 47° and with a slight angle from the bottom. Thus, the assumption of Krag et al., 2017 is confirmed.

The fact of modelling the particle impact as a manoeuvre has clearly benefited the GNSS residuals and processing parameters obtained by all solutions. Fig. 18 shows the GNSS carrier phase residuals obtained by CPOD, DLR and TUD solutions before and after a manoeuvre is modelled. As seen in the figure, the weird behaviour of the residuals shown in the vicinity of the event is corrected on every case when the particle impact is modelled. Same improvement can be observed for the case of the estimated parameters. Fig. 19 depicts an example for one of the CPR parameters estimated on the generated CPOD solution. Moreover, the drag scale factor estimated by CPOD solution on this day also improves its result from value 3.59 when no manoeuvre is modelled to value 0.92 (nominal value seen in Fig. 8) when the particle impact is modelled. Although not shown, this same behaviour is obtained for the estimated parameters of DLR and TUD solutions.

The analysis of the orbit comparisons may also be used to identify unexpected events such as the particle impact. A combined orbit solution has been generated for the case without modelling the event, and another solution has been obtained after considering a manoeuvre. Table 4 summarises the weight values given to each solution for the combination tool. Despite AIUB also generated an orbit solution for this day, this solution has been excluded for the combination to ease the comparison between generated combined solutions. When no manoeuvre is estimated, the combination tool gives more credit to CPOD and DLR solutions. The weight values are closer for all three solutions after modelling the event.

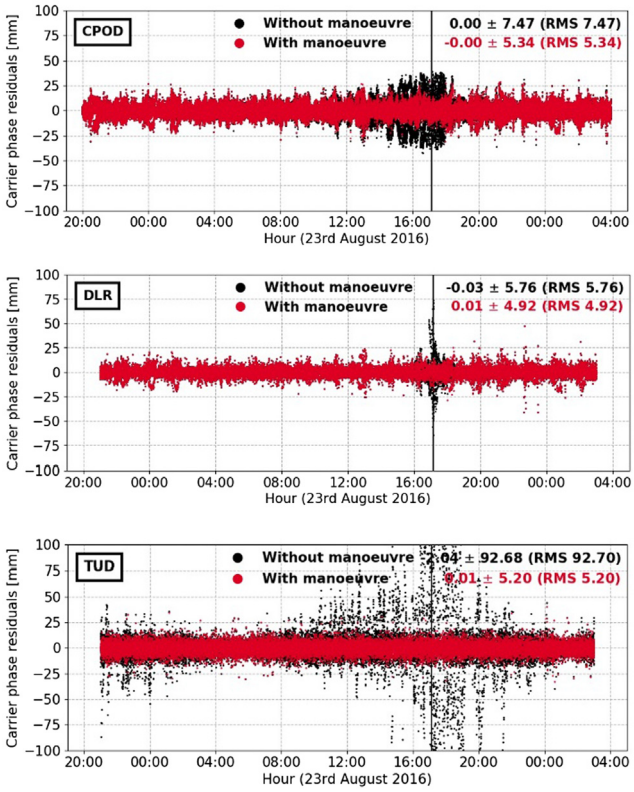

Fig. 18. Carrier phase residuals [mm] calculated by CPOD, DLR and TUD before and after modelling the particle impact as a manoeuvre on 23rd August 2016. Vertical black line correspond to the time of the manoeuvre. Mean ± STD (RMS) statistics are in mm.

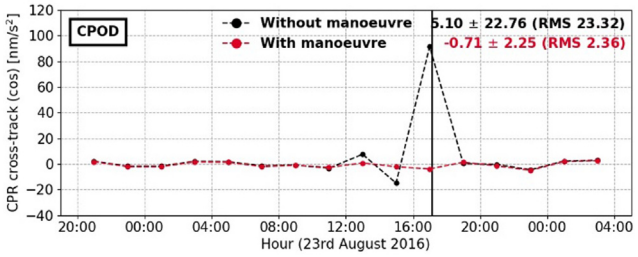

Fig. 19. Estimated CPR cosine parameters in cross-track [nm/s^2] obtained by CPOD solution before and after modelling the particle impact as a manoeuvre on 23rd August 2016. Vertical black line correspond to the time of the manoeuvre. Mean ± STD (RMS) statistics are in nm/s^2.

Table 4
Weight values [-] given to all solutions before and after modelling the particle impact as a manoeuvre on 23rd August 2016.

Manoeuvre estimated	Orbit solution			
	AIUB	CPOD	DLR	TUD
NO	None	0.396104	0.402726	0.201169
YES	None	0.389509	0.309315	0.301176

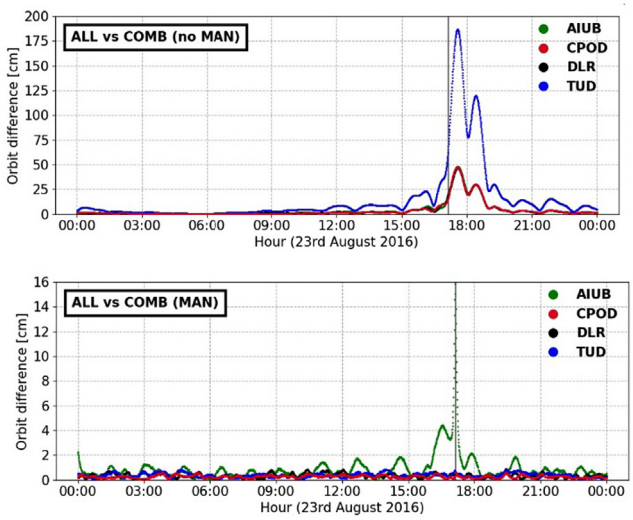

Fig. 20. Orbit differences [3D, cm] between Sentinel-1A AIUB, CPOD, DLR and TUD solutions against the combined orbit solution on 23rd August 2016 (top without modelling a manoeuvre, and bottom with a modelled manoeuvre). Vertical black line correspond to the time of the manoeuvre.

The results on the orbit comparisons shown in Fig. 20 confirm the good agreement between solutions after the modelling of the particle impact. Before doing this, the orbit solutions presented large differences between them in the vicinity of the event. Finally, the orbit comparisons of AIUB solution also obtain very close results to the combined orbit solution despite not being estimated any manoeuvre.

5. Summary and conclusion

The processing set-up improvements carried out for the Sentinel-1 satellites over the last years (e.g., change of reference frame, ARP correction, modelling updates, new orbit parametrisation, etc.) have led to perform a reprocessing campaign of the complete Sentinel-1 orbit time series. Centres of the Copernicus POD QWG have participated in this Sentinel-1 reprocessing providing their orbit solutions in addition to the official reprocessed CPOD solutions. A combined orbit solution from all these available solutions has been generated as a means of verification. Sentinel-1 satellites are not equipped by other observation techniques, and therefore, independent validation is not possible. The article has provided results of the generated combined orbit solution. The performance of all solutions contributing to the generation of this combined solution has also been analysed by either evaluating processing metrics, estimated parameters and orbit overlaps or showing the outcome of the calculated orbit comparisons against the combined orbit solution. A consistent mean value below 1 cm 3D RMS is achieved by all solutions for the entire period of time evaluated, which is a value well below the required accuracy threshold for Sentinel-1 orbit products of 5 cm in 3D RMS in comparison to external orbit products. This article has also revealed the need for further analyses to be done on the orbit solutions due to performance differences between eclipse and non-eclipse periods of the satellites.

The Copernicus POD Service has made available their reprocessed solution, replacing the former operational one, within the ESA COAH. Since 1st January 2021, the Sentinel-1 orbit products as well as the Attitude and RINEX file products are routinely made available for the overall Sentinel-1 mission (same for Sentinel-2 and -3 missions) through this channel.

Declaration of Competing Interest

The authors declare that they have no known competing financial interests or personal relationships that could have appeared to influence the work reported in this paper.

Acknowledgements

The Copernicus POD Service is financed under ESA contract No. 4000132155/21/I-BG, which is gratefully acknowledged. The work performed in the frame of this contract is carried out with funding by the European Union. The views expressed herein can in no way be taken to reflect the official opinion of either the European Union or the European Space Agency.

Appendix A. See Table A1–A3.

Table A1
List of offsets of observation epochs different from exact multiples of 10 (entries in italic are time intervals from the redundant receiver).

Offset	from	to	Offset	from	to
Sentinel-1A			*Sentinel-1B*		
5	06/04/2014, 01:16:35.000	03/09/2014, 07:56:25.000	9	27/04/2016, 04:43:29.000	17/04/2019, 23:27:29.000
8	03/09/2014, 17:09:18.000	10/05/2015, 02:37:28.000	8	18/04/2019, 15:45:58.000	today
2	10/05/2015, 14:01:12.000	07/06/2015, 05:30:02.000			
4	07/06/2015, 11:10:14.000	28/06/2015, 15:55:44.000			
7	28/06/2015, 19:18:17.000	06/072015, 08:45:17.000			
5	06/07/2015, 11:12:25.000	28/07/2015, 10:40:55.000			
5	*28/07/2015, 10:41:05.000*	*03/082015, 01:40:05.000*			
2	03/08/2015, 14:46:52.000	03/082015, 17:48:02.000			
9	04/08/2015, 12:14:59.000	12/08/2015, 09:26:29.000			
6	*12/08/2015, 09:26:46.000*	*14/09/2015, 13:53:06.000*			
5	14/09/2015, 13:53:15.000	18/04/2019, 00:17:45.000			
4	18/04/2019, 14:57:54.000	today			

Table A2
Sentinel-1A and Sentinel-1B orbit overlaps filtered out from the statistics as a result of large gaps of L0 data between consecutive days.

Orbit solution	Satellite	Day/s
AIUB	S-1A	11/10/2014, 21/06/2015, 28/07/2015([1]), 03/08/2015[(1)], 04/08/2015, 05/08/2015, 10/08/2015, 05/09/2015, 15/09/2015[(1)], 08/11/2015, 22/02/2016, 25/11/2016, 02/06/2018, 01/03/2020
	S-1B	06/05/2016, 29/06/2016, 29/06/2019
CPOD	S-1A	11/10/2014, 30/12/2014, 02/02/2015, 20/02/2015, 21/06/2015, 04/08/2015, 05/08/2015, 10/08/2015, 05/09/2015, 06/11/2015, 08/11/2015, 11/12/2015, 22/02/2016, 25/11/2016, 02/06/2018, 01/03/2020
	S-1B	29/04/2016, 06/05/2016, 29/06/2016, 18/04/2019, 29/06/2019
DLR	S-1A	11/10/2014, 30/12/2014, 06/11/2015, 08/11/2015, 02/06/2018, 01/03/2020
	S-1B	29/06/2016, 18/04/2019, 29/06/2019
TUD	S-1A	02/06/2018, 01/03/2020
	S-1B	18/04/2019, 29/06/2019

[(1)] Day combining data from nominal and redundant receivers. The processing of AIUB solution did not use the data from both receivers together. The data from one of the receivers is consequently omitted, and the solution is processed including a large gap of L0 data.

Table A3
Sentinel-1A and Sentinel-1B orbit solutions not used for the combination due to orbit gaps at the beginning or end of the solution (other reasons are detailed within the table).

Orbit solution	Satellite	Day/s
AIUB	S-1A	28/07/2015[(1)], 03/08/2015[(1)], 14/09/2015[(1)], 23/08/2016[(2)]
DLR	S-1A	29/05/2014, 02/06/2014, 02/02/2015, 20/02/2015, 20/06/2015, 21/06/2015, 28/07/2015, 04/08/2015, 05/08/2015, 10/08/2015, 05/09/2015, 11/12/2015, 22/02/2016, 25/11/2016, 18/04/2019[(3)]
	S-1B	03/05/2016[(4)], 06/05/2016, 09/05/2016, 13/05/2016, 21/05/2016, 23/05/2016, 30/05/2016, 01/06/2016, 04/06/2016, 06/06/2016, 18/04/2019[(3)]
TUD	S-1A	29/05/2014, 02/06/2014, 05/07/2014, 07/07/2014, 29/12/2014, 30/12/2014, 01/02/2015, 02/02/2015, 19/02/2015, 20/02/2015, 17/03/2015[(4)], 20/06/2015, 21/06/2015, 03/08/2015, 04/08/2015, 09/08/2015, 10/08/2015, 13/08/2015, 04/09/2015, 05/09/2015, 05/11/2015, 06/11/2015, 07/11/2015, 08/11/2015, 10/12/2015, 11/12/2015, 21/02/2016, 22/02/2016, 24/11/2016, 25/11/2016
	S-1B	28/04/2016, 29/04/2016, 05/05/2016, 06/05/2016, 09/05/2016, 13/05/2016, 21/05/2016, 23/05/2016, 30/05/2016, 01/06/2016, 04/06/2016, 06/06/2016, 28/06/2016, 29/06/2016

[(1)] Day combining data from nominal and redundant receivers. The processing of AIUB did not use the data from both receivers together. The data from one of the receivers is consequently omitted, and the solution is processed including a large gap of L0 data leading to large differences with respect to the other solutions.
[(2)] Day of the particle impact on Sentinel-1A satellite (see Section 4.4). AIUB solution has been excluded to the combination since it is the only solution non-estimating a manoeuvre on this day.
[(3)] Day with a large gap of L0 data. The solution shows higher orbit differences than expected with respect to the others out of the interval of time of the gap of L0 data.
[(4)] Solution presenting higher orbit differences than expected with respect to the others without any event (gap or manoeuvre) occurring during this day.

References

Allahvirdi-Zadeh, A., Wang, K., El-Mowafy, A., 2022. Precise Orbit Determination of LEO Satellites Based on Undifferenced GNSS Observations. J. Surv. Eng. 148(1), art.03121001, 10.1061/(ASCE)SU.1943-5428.0000382.

Aschbacher, J., Milagro-Pérez, M., 2012. The European Earth monitoring GMES programme: Status and perspectives. Remote Sens. Environ. 120, 3–8. https://doi.org/10.1016/j.rse.2011.08.028.

Bertiger, W., Bar-Sever, Y., Dorsey, A., et al., 2020. GipsyX/RTGx, a new tool set for space geodetic operations and research. Adv. Space Res. 66, 469–489. https://doi.org/10.1016/j.asr.2020.04.015.

Beutler, G., Kouba, J., Springer, T.A., 1995. Combining the orbits of the IGS Analysis Centers. Bulletin Géodésique 69, 200–222. https://doi.org/10.1007/BF00806733.

Bruinsma, S., Thuillier, G., Barlier, F., 2003. The DTM-2000 empirical thermosphere model with new data assimilation and constraints at lower boundary: accuracy and properties. J. Atmos. Solar-Terrestrial Phys. 65, 1053–1070. https://doi.org/10.1016/S1364-6826(03)00137-8.

Dach, R., Schaer, S., Arnold, D., et al., 2020. CODE final product series for the IGS, Published by Astronomical Institute, University of Bern (URL: http://www.aiub.unibe.ch/download/CODE). http://dx.doi.org/10.7892/boris.75876.

Dach, R., Lutz, S., Walser, P. Fridez (Eds.), 2015. Bernese GNSS Software Version 5.2. Astronomical Institute, University of Bern, Bern Open Publishing (ISBN: 978-3-906813-05-9). http://dx.doi.org/10.7892/boris.72297.

Dobslaw, H., Dill, R., Dahle, C., 2018. GRACE Geopotential GAA Coefficients GFZ RL06. V. 6.0. GFZ Data Services. https://doi.org/10.5880/GFZ.GRACE_06_GAA

Duan, B., Hugentobler, U., 2021. Comparisons of CODE and CNES/CLS GPS satellite bias products and applications in Sentinel-3 satellite precise orbit determination. GPS Sol. 25, 128. https://doi.org/10.1007/s10291-021-01164-5.

Fernández, J., Calero, E., Peter, H., Féménias, P., 2019. Copernicus POD Service: Reprocessing of the Copernicus Sentinel-1, -2, -3 orbits. Geophys. Res. Abstracts 21, EGU2019-8946, EGU General Assembly 2019 .

Fernández, J., Escobar, D., Águeda, F., Féménias, P., 2014. Sentinels POD Service Operations. In: SpaceOps 2014 Conference, SpaceOps Conferences, AIAA 2014-1929. https://doi.org/10.2514/6.2014-1929.

Fiedler, H., Börner, E., Mittermayer, J., Krieger, G., 2005. Total zero Doppler steering – a new method for minimizing the Doppler centroid. IEEE Geosci. Remote Sens. Lett. 2 (2), 141–145. https://doi.org/10.1109/LGRS.2005.844591.

Fletcher, K. (Ed.), 2012. Sentinel-1: ESAs Radar Observatory Mission for GMES Operational Services. ESA SP-1322/1, ESA Communications (ISBN: 978-92-9221-418-0).

Förste, C., Flechtner, F., Schmidt, R. et al., 2006. A mean global gravity field model from the combination of satellite mission and altimetry/gravimetry surface data. Poster presented at EGU General Assembly 2006. Geophys. Res. Abstracts. Vol.8, 03462.

Folkner, W.M., Williams, J.G. and Boggs, D.H., 2009. The Planetary and Lunar Ephemeris DE421. JPL Interplanetary Network Progress Report 42-178 (http://ipnpr.jpl.nasa.gov/progress_report/42-178/178C.pdf). Last access: 17 Sep 2021.

GMES Sentinel-1 Team, 2010. GMES Sentinel-1 System Requirements Document, Iss. 3/Rev. 3, ESA-ESTEC technical note Ref. S1 RS ESA SY 0001, 143p.

GMV, 2021. Regular Service Review Reports (https://sentinels.copernicus.eu/web/sentinel/technical-guides/sentinel-1-sar/pod/documentation) => Regular Service Review (last access: 17 Sep 2021).

Hedin, A.E., 1991. Extension of the MSIS Thermosphere Model into the middle and lower atmosphere. J. Geophys. Res. 96 (A2), 1159–1172. https://doi.org/10.1029/90JA02125.

van den Ijssel, J., Forte, B., Montenbruck, O., 2016. Impact of Swarm GPS receiver updates on POD performance. Earth Planets Space 68, 85. https://doi.org/10.1186/s40623-016-0459-4.

Johnston, G., Riddell, A., Hausler G., 2017. The International GNSS Service. In: Teunissen, Peter J.G., Montenbruck, O. (Eds.). Springer Handbook of Global Navigation Satellite Systems, 1st ed., Springer International Publishing, Cham, Switzerland, pp. 967-982. https://doi.org /10.1007/978-3-319-42928-1.

Kobel, C., Arnold, D., Jäggi, A., 2019. Combination of precise orbit solutions for Sentinel-3A using Variance Component Estimation. Adv. Geosci. 50, 27–37. https://doi.org/10.5194/adgeo-50-27-2019.

Krag, H., Serrano, M., Braun, V., et al., 2017. A 1 cm space debris impact onto the Sentinel-1A solar array. Acta Astronautica 137, 434–443. https://doi.org/10.1016/j.actaastro.2017.05.010.

Lazecky, M., Hooper, A., 2022. InSAR-derived horizontal velocities in a global reference frame. In: ESSOAr (preprint). https://doi.org/10.1002/essoar.10511058.1 (URL: https://www.essoar.org/doi/pdf/10.1002/essoar.10511058.1)

Lemoine, J.-M-, Biancale, R., Reinquin, F. et al., 2019. CNES/GRGS RL04 Earth gravity field models, from GRACE and SLR data. GFZ Data Services. https://doi.org/10.5880/ICGEN.2019.010.

Louet, J., 2001. The Envisat Mission and System. ESA Bulletin No.106 (EnviSat Special Issue), pp.10-25 (http://www.esa.int/esapub/bulletin/bullet106/bul106_1.pdf). Last access: 17 Sep 2021.

Lyard, F.H., Allain, D.J., Cancet, M., et al., 2021. FES2014 global ocean tides atlas: design and performance. Ocean Sci. 17, 615–649. https://doi.org/10.5194/os-17-615-2021.

Lyard, F., Lefèvre, F., Letellier, T., Francis, O., 2006. Modelling the global ocean tides: modern insights from FES2004. Ocean Dyn. 56, 394–415. https://doi.org/10.1007/s10236-006-0086-x.

Mao, X., Arnold, D., Girardin, V., et al., 2021. Dynamic GPS-based LEO orbit determination with 1 cm precision using the Bernese GNSS Software. Adv. Space Res. 67, 788–805. https://doi.org/10.1016/j.asr.2020.10.012.

Martin Serrano, M.A., Shurmer, I., Marc, X., 2012. Sentinel-1: operational approach to the orbit control strategy. In: Proceedings 23th International Symposium on Space Flight Dynamics – 23th ISSFD, Pasadena, US.

Miranda, N., 2015. Sentinel-1 Instrument Processing Facility. Technical Note. ESA-EOPG-CSCOP-TN-0004 (https://sentinel.esa.int/documents/247904/1653440/Sentinel-1-IPF_EAP_Phase_correction). Last access: 17 Sep 2021.

Montenbruck, O., Hackel, S., Wermuth, M., Zangerl, F., 2021. Sentinel-6A precise orbit determination using a combined GPS/Galileo receiver. J. Geod. 95, art.109. https://doi.org/10.1007/s00190-021-01563-z.

Montenbruck, O., Hackel, S., Jäggi, A., 2018. Precise orbit determination of the Sentinel–3A altimetry satellite using ambiguity-fixed GPS carrier phase observations. J. Geod. 92, 711–726. https://doi.org/10.1007/s00190-017-1090-2.

Pail, R., Goiginger, H., Schuh, W.-D., et al., 2010. Combined satellite gravity field model GOCO01S derived from GOCE and GRACE. Geophys. Res. Lett. 37 (20). https://doi.org/10.1029/2010gl044906.

Peter, H. and GMV team, 2021. POD Product Handbook (https://sentinels.copernicus.eu/web/sentinel/technical-guides/sentinel-1-sar/pod/documentation) => POD Product Handbook (last access: 17 Sep 2021).

Peter, H., Fernández, J., Féménias, P., 2020a. Copernicus Sentinel-1 satellites: sensitivity of antenna offset estimation to orbit and observation modelling. Adv. Geosci. 50, 87–100. https://doi.org/10.5194/adgeo-50-87-2020.

Peter, H., Berzosa, J, Fernández, M. et al., 2020b. Copernicus POD Service - Evolutions in Sentinel-3 Orbit Determination. Presented at POD splinter of virtual OSTST 2020, October 19-23, 2020.

Peter, H., Berzosa, J., Fernández, J., Féménias, P., 2020c. Long-term evaluation of estimated solar radiation pressure coefficients from Copernicus Sentinel-1, -2, -3 satellites. EGU General Assembly 2020, online. 4-8 May 2020. EGU2020-5288. https://doi.org/10.5194/egusphere-egu2020-5288.

Peter, H., Jäggi, A., Fernández, J., et al., 2017. Sentinel-1A - First precise orbit determination results. Adv. Space Res. 60, 879–882. https://doi.org/10.1016/j.asr.2017.05.034.

Petit, G., Luzum, B., 2010. IERS Conventions (IERS Technical Note 36). Frankfurt am Main: Verlag des Bundsamtes für Kartogrphie und Geodäsie (ISBN 3-89888-9898-6). Last access: 17 Sep 2021.

Picone, J.M., Hedin, A.E., Drob, D.P., Aikin, A.C., 2002. NRLMSISE-00 empirical model of the atmosphere: Statistical comparisons and scientific issues. J. Geophys. Res. 107 (A12). https://doi.org/10.1029/2002JA009430.

Rebischung, P., 2020. Switch to IGb14 reference frame, IGSMAIL-7921, 14th April 2020. https://lists.igs.org/pipermail/igsmail/2020/007917.html (last access: 17 Sep 2021).

Rebischung, P., 2016. Upcoming switch to IGS14/igs14.atx, IGSMAIL-7399, 21st December 2016. https://lists.igs.org/pipermail/igsmail/2016/007399.html (last access: 17 Sep 2021).

Rebischung, P, Schmid, R., 2016. IGS14/igs14.atx: a new framework for the IGS products. AGU Fall meeting, San Francisco CA, G41A-0998.

Romero, I., 2020. RINEX – the receiver independent exchange format, v.3.05, 1st December 2020. https://files.igs.org/pub/data/format/rinex305.pdf (last access: 17 Sep 2021).

Rothacher, M., Schmid, R., 2010. ANTEX: The Antenna Exchange Format, Version 1.4. 15th September 2010. https://kb.igs.org/hc/en-us/articles/216104678-ANTEX-format-description (last access: 17 Sep 2021).

Savcenko, R., Bosch, W., Dettmering, D., Seitz, F., 2012. EOT11a – Global Empirical Ocean Tide model from multi-mission satellite altimetry, with links to model results. PANGAEA. https://doi.org/10.1594/PANGAEA.834232.

Schaer, S., Villiger, A., Arnold, D., et al., 2021. The CODE ambiguity-fixed clock and phase bias analysis products: generation, properties, and performance. J. Geod. 95, art.81. https://doi.org/10.1007/s00190-021-01521-9.

Springer, T.A., Dilssner, F., Escobar, D. et al., 2011. NAPEOS: The ESA/ESOC tool for Space Geodesy. Geophysical Research Abstracts, Vol. 13, EGU2011-8287, EGU General Assembly 2011.

Standish, E.M., 1998. JPL Planetary and Lunar Ephemerides, DE405/LE405. Interoffice memorandum. JPL IOM 312, F-98-048.

Steigenberger, P., Thölert, S., Montenbruck, O., 2019. Flex power on GPS Block IIR-M and IIF. GPS Sol. 23, art.8. https://doi.org/10.1007/s10291-018-0797-8.

Torres, R., Snoeij, P., Geudtner, D., et al., 2012. GMES Sentinel-1 mission. Remote Sens. Environ. 120, 9–24. https://doi.org/10.1016/j.rse.2011.05.028.

Villiger, A., Dach, R., Arnold, D., et al., 2020. CODE repro3-IGb14 product series. Astronomical Institute, University of Bern. https://doi.org/10.48350/146753.

Wermuth, M., Montenbruck, O., van Helleputte, T., 2010. GPS high precision orbit determination software tools (GHOST). IN: 4th International conference on astrodynamics tools and techniques, 3-6 May 2010, Madrid.

Wu, S.C., Yunck, T.P., Thornton, C.L., 1991. Reduced-dynamic technique for precise orbit determination of low earth satellites. J. Guid. Control Dyn. 14, 24–30. https://doi.org/10.2514/3.20600.

Zangerl, F., Griesauer, F., Sust, M., et al., 2014. SWARM GPS precise orbit determination receiver initial in-orbit performance evaluation. In: 27th International Technical Meeting of the Satellite Division of the Institute of Navigation, ION GNSS 2014. Vol. 2, pp. 1459–1468.